Yb-YAG laser offset welding of AA5754 and T40 butt joint

Fiber laser welding of Al5754 and T40 dissimilar butt joint

Giuseppe Casalino[a], Michelangelo Mortello[a], Patrice Peyre[b]

[a] Dipartimento di Meccanica, Matematica e Management, Viale Japigia 182, Bari 70126, Italy

[b] PIMM Laboratory, UMR 8006 CNRS, Arts et Métiers ParisTech, 151 Bd de l'Hôpital, 75013 Paris, France

Abstract

Joining processes of various materials with titanium are difficult to perform by conventional techniques because of both the presence of a tenacious oxide coating on its surface and because of a limited Ti solubility with other elements. In this work, laser welding of Al5754 and T40 dissimilar butt weld was performed by focusing the laser beam on the titanium side, which provokes a key-hole in the Ti and the heat conduction melting of the aluminum side. No filler metal or grooves preparation were used. The effects of welding conditions on the intermetallic layer, which forms during the heat conduction welding of aluminum to titanium, were studied. Microstructure was analyzed through optical inspections, chemical analyses and Vickers micro-hardness tests. It was obtained a narrow intermetallic layer (IM) along the Ti/Al interface whose morphology was either planar or undulated, depending on the physical state of the titanium close to the interface at the moment of the aluminum fusion. Sound welds together with a good robustness of the laser welding process were obtained.

1. Introduction

Dissimilar lightweight structures of Ti/Al alloys have several potential applications in aerospace and automotive industries. The applications of these two materials have had a large increase. Miller et al. (2000) and Faller et al. (2001) summarized the development of aluminum and titanium alloys for several automotive applications. Dissimilar structures offer attractive features in comparison with

homogeneous materials. Different joining mechanisms are available to produce efficient hybrid structures. Mechanical joining processes such as riveting, clinching, and screwing are currently the most widely used techniques to achieve connection between different materials because they are not dependent on the metallurgical compatibility. In fact, the reaction between two different materials at high temperatures leads to the formation of intermetallic compounds and the efficiency of the assembly depends on their chemical and thermal affinity. Different intermetallic compounds form during the joining process and different characteristics are associated to each one. Bondar et al. (2011) conducted a chemical and mechanical analysis on several intermetallic Al-Ti compounds in term of strength and plasticity. A sound weld of aluminum to titanium alloy is difficult mainly because of the strong difference in crystal microstructure, physical and thermochemical properties. Solid state welding techniques have been adopted in previous researches. The formation of intermetallic compounds occurs both in the solid state and fusion welding. Luo and Acoff (2000) conducted an investigation on diffusion welded multi-laminated composites of Ti and Al and showed that the $TiAl_3$ intermetallic compound forms in relatively short times and at temperatures of about 660-680°C. Dressler et al. (2009) conducted a study on FSW of dissimilar Al-Ti joints by shifting the tool pin center towards the aluminum plate. However some particles in the stirred zone of the Al side were found and this lead to the formation of cavities during the tensile tests. Moreover, Chen et al. (2011) pointed out the difficulties in performing butt welds by FSW because of the tendency to cracks and grooves, especially when the tool rotation rate of stir head is too high.

Finally, as concerns the interaction between the laser source and the alloys some researches showed some encouraging results at fusion welding of titanium and aluminum alloys. Squillace et al. (2012) optimized the laser beam welding of Ti6Al4V alloy and showed how to control and improve the quality of joints both in key-hole and heat conduction laser welding. While Akman et al. (2009) executed the process in pulsed mode and demonstrated how to control the welding by varying the ratio between pulse energy and pulse duration.

Although many authors performed experimental analysis of the laser beam welding of aluminum alloys, several problems have not understood, yet. As discussed by Pastor et al. (1999), several harmful phenomena happen during the laser beam welding of aluminum alloys. The collapse of the key-hole and the turbulent flow in the weld pool cause the entrapment of the gas bubbles, which derive from the vaporized alloy elements, the shielding gases and the environmental air, and generate porosity. Moreover, loss of volatile alloying elements with a low vaporization point, such as magnesium and zinc, causes the degradation of mechanical properties of the solid-solution strengthened alloy. Kuo and Lin (2006) showed that hot cracking and porosity provoke a significant reduction of the mechanical properties. Haboudou et al. (2003) demonstrated that surface preparation reduces the hydrogen source responsible of the microporosity but the problem of gases suppression is yet unsolved. Among the laser welding of aluminum alloy, it is worth to remember the recent work of Casalino et al. (2014). In that work the authors demonstrated that the combination of the fiber laser and the arc welding source favors the stability of the process and provides good structural and geometrical properties of the weld.

Most of the studies on the Al-Ti laser welding have been conducted in the key-hole welding mode by positioning the laser spot on the aluminum side (Alfieri et al. 2013). Chen et al. (2010) found that insufficient interfacial reaction favors crack initiation and thick continuous layer leads to an increase of embrittlement and spontaneous crack initiation during welding. Song et al. (2013) studied the process to perform butt welds by focusing the laser beam on the aluminum alloy. It was shown that the increase laser offset reduces the thickness of interfacial layer and improves mechanical properties and microstructure. Nevertheless, the local heating during the process leads to interfacial non-homogeneity and to a reduction in the joint quality. Chen et al. 2011 studied the interfacial reaction non-homogeneity during laser welding-brazing. They used a circular laser spot with Gaussian energy distribution that favored the stability of the process and prevented heterogeneous interfacial reaction. Nevertheless, certain aspects concerning the formation and growth of the interface reaction non-homogeneity and diffusion mechanisms are not fully clear yet. For the above-mentioned difficulties,

the focalization of the source on the aluminum side has resulted to be far from a suitable solution for joining Ti and Al. Recently, fiber laser-cold metal transfer arc hybrid welding was developed to join a Ti6Al4V Ti alloy to an AA6061 Al alloy in butt configuration by Ming Gao et al. 2014.

In the present study, the laser welding of Al5754 aluminum alloy and T40 titanium alloy was investigated. Unlike most of the previous studies, the laser beam was focused on the titanium side. Differently than Möller et al. (2011), autogenous laser welding was used. The key-hole laser fusion of the titanium was more stable and regular than that of the aluminum and the porosity problems were overcome, which improves the robustness of the process. The investigation gave a special attention to the interfaces, which generated during the welding process. Either Ti heat affected zone and Al liquid or Ti to Al liquid interface formed, which depended on the process parameters. The effects of welding conditions on both the intermetallic layers, which form during the welding process, were studied through optical inspections, chemical analyses and Vickers micro-hardness test. The tensile test and the analysis of the rupture surfaces complete this investigation.

Eventually, this paper demonstrates that focusing the laser on the Ti side is a promising approach to the production of sound and robust Ti/Al assemblies.

2. Experimental procedure

2.1 Materials properties and samples preparation

In this work T40 alloy and Al5754 alloy plates with thickness of 1.5 mm were used for assemblies. Tables 1, 2 and 3 show the chemical composition, mechanical properties and thermo-physical properties of the two alloys considered.

Table 1
Chemical composition of the as-received materials.

	Ti	Al	H	Mg	Fe	Mn	Si	Cr	O	Cu	N	C

T40	balance	-	<0.015	-	<0.03	-	-	-	<0,25	-	<0.03	<0.1
Al5754	<0.15	balance	-	2.6-3.6	0.40	0.50	0.40	0.30	-	0.10	-	-

Table 2
Mechanical properties of the as-received materials.

	UTS (MPa)	**YS (MPa)**	**E (GPa)**	**A%**	**HV**
T40	460	276	105	20	145
Al5754	230	80	68	17	62

Table 3
Thermo-physical properties of the two base materials.

	K (W/(m.K))	**Tm (k)**	**ρ (g/ cm ^{3})**
T40	17	1930	4.51
Al5754	147	870	2.66

Prior to welding, the interface surfaces were saw-cut at low speed (1-3 mm/s) and polished with a 200 grit sandpaper in order to minimize roughness and limit thermal contact resistance between the two sheets. Moreover, roughness was determined on lateral sides. Figures 1(a) and 1(b) show two examples of roughness profile detected on the contact surface of the titanium side and aluminum side respectively before the butt-welding tests. Average roughness Ra was shown to be nearly 0.9 μm on the Ti side and 2.4 μm on the Al side. Ry is the value of the peak height of the roughness profile. That of the Ti sheet resulted to be about the 20% of that detected for the Al (Fig 1). While Rq, is defined as the mean square of the deviations of height from the average height. For the Al the Rq revealed a greater fluctuation in height for Al respect to Ti (Fig. 1).

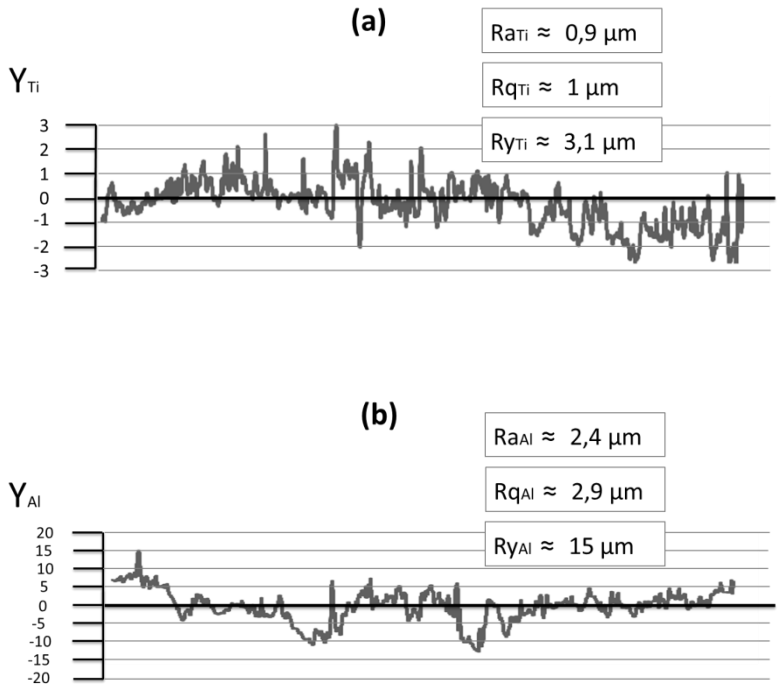

Fig.1. Roughness profile of the interface (a) titanium alloy and (b) aluminum alloy.

As described by the curves, the roughness achieved for the titanium alloy results to be greater than that detected for the aluminum sheet because of its greater hardness. In fact at the aluminum surface share peaks reach values of about ±15µm while at the titanium side the values registered are only ±3mm. This depends on the fact that on the aluminum surface, that is softer, cutting forces during the smoothing produce a more non-homogeneous removal rate. So the roughness detected for the titanium alloy has resulted to worth about the 40% of that detected for the aluminum sheet. The microstructure and the geometry of the interfacial layer strictly depend on the contact condition, which becomes a critical issue.

2.2 Laser equipment and welding set-up

A Yb-YAG laser (±0.3 µm), was used in continuous wave regime with maximal output powers of 3 kW (2). The laser beam, delivered to the work station via an optical fiber of 200 µm diameter, was focused through an optical head composed of a collimating lens and a focusing lens with a focal length of 200 mm. A slight defocusing (-2 mm) was used, resulting in an approximately 300 µm

diameter near-Gaussian distribution. Both top and bottom surface of the sheets were shielded using Argon gas with a flow rate of 20 l/min. Laser beam spot was focused on the top surface of the titanium alloy plate with an offset between the center of the laser spot and the interface variable from 0.5 mm and 1.4 mm. The welding system is shown schematically in figure 2.

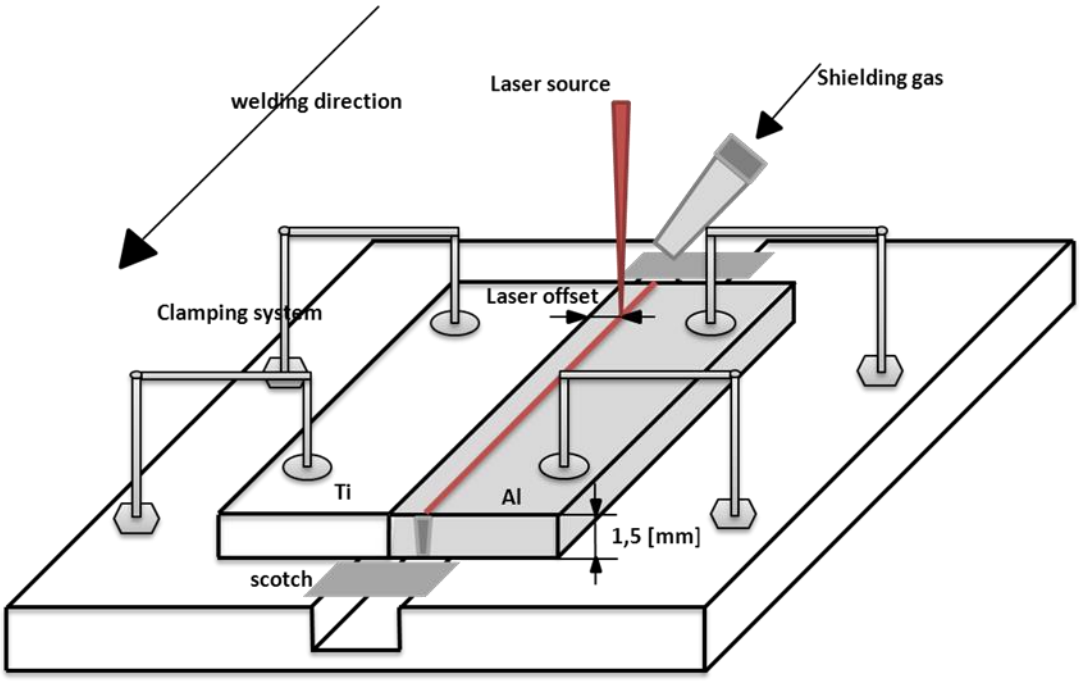

Fig. 2. Set-up of the welding system.

2.3 Process parameters

Preliminary experimental tests and two experimental plans were carried out. Table 4 and 5 show the process parameters determined according to preliminary tests and adopted to carry out the analysis. During the first experimental campaign the laser offset was taken constant (equal to 0.75 mm) in order to assess the specific effect of the lineic energy on welds characteristics. Subsequently, a reduction of the lineic energy (P(W)/ V(mm/s)) for various laser offsets was adopted to try to reduce the adverse effects of the laser beam source on the geometric and metallurgical properties of the welds.

Table 4
Process parameters adopted for the first experimental plan.

Sample	Laser power (kW)	Welding speed (m/min)	Laser offset Δx (mm)	Lineic energy (J/mm)
1	1.5	1.6	0.75	56,24
2	2	1.8	0.75	66.67
3	1.75	2	0.75	52.50
4	1.75	1.8	0.75	58.33
5	1.5	2	0.75	45.00
6	1.5	1.8	0.75	50.00
7	2	2	0.75	60.00
8	2	1.6	0.75	75.00
9	1.75	1.6	0.75	65.62

Table 5
Process parameters adopted for the second experimental plan.

Sample	Laser power (kW)	Welding speed (m/min)	Laser offset (mm)
10	1.5	2.5	0.75
11	1.5	2.5	0.5
12	1.5	3	0.5
13	1.5	3	0.75

2.4 Weld characterization procedure

The joints were cross-sectioned perpendicularly to the welding direction then polished and chemically etched in order to analyze the microstructures. Keller's reagents solution (1% HF, 1.5% HCl, 2.5% HNO_3 and 95% H_2O) was used to optimize the observation. Microstructures were analyzed with optical microscopy (OM) and scanning electron microscopy (SEM) equipped with energy-dispersive X-ray spectrometer (EDS) to analyze the chemical composition close to the interface between the two materials. Last, tensile tests were conducted using the INSTRON 5881 machine (figure 3) with a 10^{-4} s^{-1}strain rate. Three specimens for each welding condition were tested (as shown in figure 4) in order to evaluate the process robustness.

Fig. 3: Tensile strength machine.

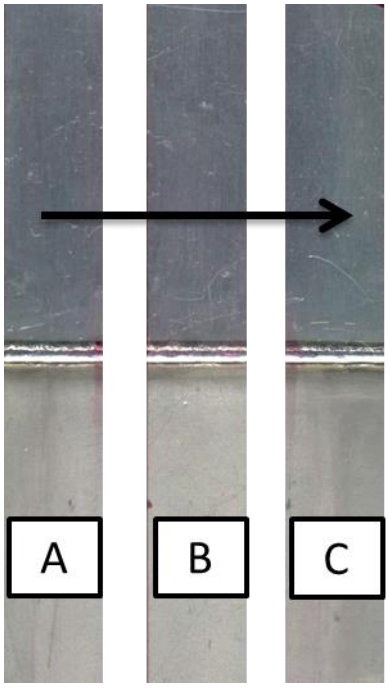

Fig. 4: Specimens studied for each welding condition.

Vickers micro-hardness profile were carried out with a 400 g load. Measurements were performed at the mid thickness of the joint and with a 0.25 mm distance between two successive imprints.

3. Results and discussion

3.1 Weld appearance

The morphology of the top and bottom surfaces of beads are shown in figures 5(a) and 5(b).

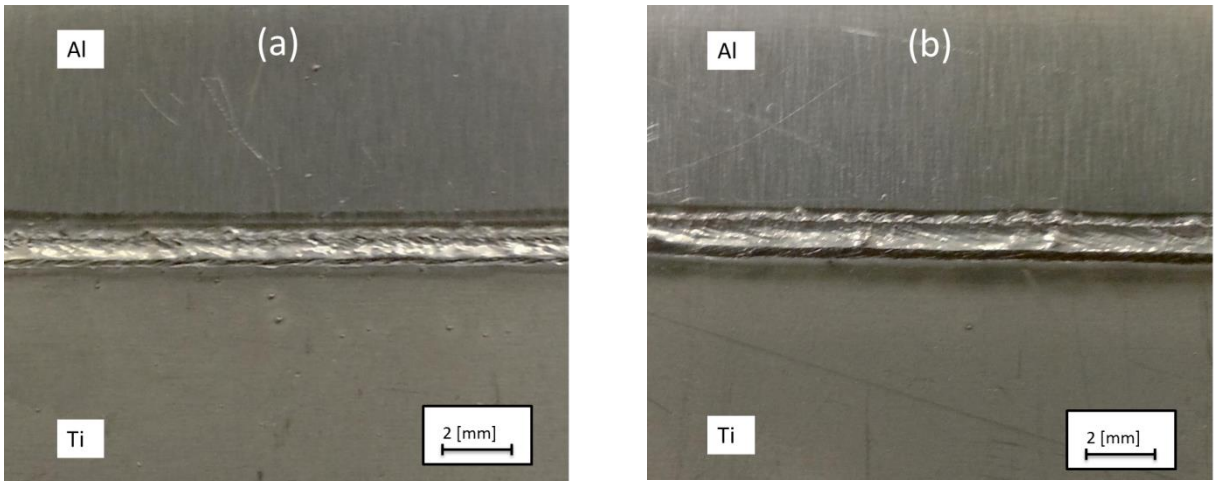

Fig. 5. Joint 6 (1.5 kW-1.8m/min-0.75mm) observed at the (a) top and (b) bottom surface.

The surface aspect was shown to be satisfactory and the amount of spatter was very low in comparison with preliminary results obtained when focusing the laser beam on the Al side. In turn, the bead resulted to be globally more homogeneous and stable than with key-holes positioned on the Al side. The region close to the interface exhibited a dark color because of the vaporization and resulting condensation of small nanometer-size particles in key-hole regime. In spite of the great affinity of Ti with oxygen, the local Ar gas shielding was shown to be efficient to limit oxidation phenomena. The width of the seam was shown to be in the 1.5-2 mm range, and it was almost similar at the top and bottom surface of beads.

3.2 Microstructural characterization

Figures 6(a), 6(b), 6(c) and 6(d) show the microstructures obtained on several samples, with optical microscopy (OM). When varying the welding conditions and parameters, different kinds of microstructure were observed. Cross sections of samples 5 and 3 are presented in the figures 6(a) and 6(b) respectively. Sample 3 was performed with a greater laser power than that for sample 5 (1.75 kW versus 1.25 kW), but for similar laser offset (0.75 mm) and welding speed (2 m/min). Logically, the lineic energy P/V (J/m) made the fusion zone larger and more prone to contacting interfacial area. As a consequence, the interface layer observed for sample 5 resulted to be straight revealing a (solid

titanium / liquid aluminum) interaction, while that observed for sample 3 was curved and discontinuous indicating mostly that Titanium was at a liquid state near the interface. Therefore, depending on the main process parameters, the interface was shown to be linear when contacting the HAZ of Ti or curvilinear when included in the Ti fusion zone (FZ). Considering that the first part of the study was carried out with a constant value of the laser offset (tab. 4), the lineic energy resulted to be the key factor for the distinction between the two types of welds described here above. As shown in figure 6b, higher heat input favored the formation of titanium agglomerates in the aluminum FZ, due to the direct liquid-liquid interaction and the occurrence of convection flow. After solidification, agglomerates of Ti remained in the Al side, but did not solubilize in the Aluminum solid solution, due to the non-solubility of Ti with Al. Figure 6a shows that Ti HAZ in the gap between the interface layer and melted Ti hindered both the Ti flows and Al flows. Therefore, melted Al, that is less viscous, crept over the top and the bottom surface of the Ti sheet. Also, small Ti agglomerates could be observed in the Al side of the joint distant from the interface as can be seen in figure 6a. These are probably due to spatters of melted Ti that felt down on the Al sheet during its solidification and remained incorporated in the Al structure, or to convection flows that pushed molten Ti inside Al FZ. Reductions in section both in the Ti side and Al side were observed. The first (in the Ti sheet) was due to the key-hole formation and the Ti/Al adhesion forces, which prevented the molten Ti from flowing towards the Al side. This resulted in a shrinkage of the sheet. Also, in the Al side, reductions of section occurred. This was probably due to the creep of Al on the Ti, which was described above. Figure 6(c) shows the cross section of a specimen obtained using low values for the laser offset and the specific heat input. Because of the low value of laser offset, the Ti FZ reached the intermetallic interface leading to a curvilinear and non-homogeneous interface layer. Moreover, the amount of heat conducted to the Al alloy was shown to be too high. This led to the formation of macro-porosities in the Al sheet side, which reduced drastically the weld properties. The microstructure of Ti after the welding is shown in figure 6d. A coarse acicular phase (α_1 Martensite phase) was evidenced in FZ, due to the fast quenching of liquid Ti. Former β grains boundaries were also shown oriented in the

direction of the heat flow (Fig. 6(d)). The main difference between HAZ and FZ was shown to be the size of a phase, which was shown to be much smaller and more equiaxe in the HAZ, that in the FZ.

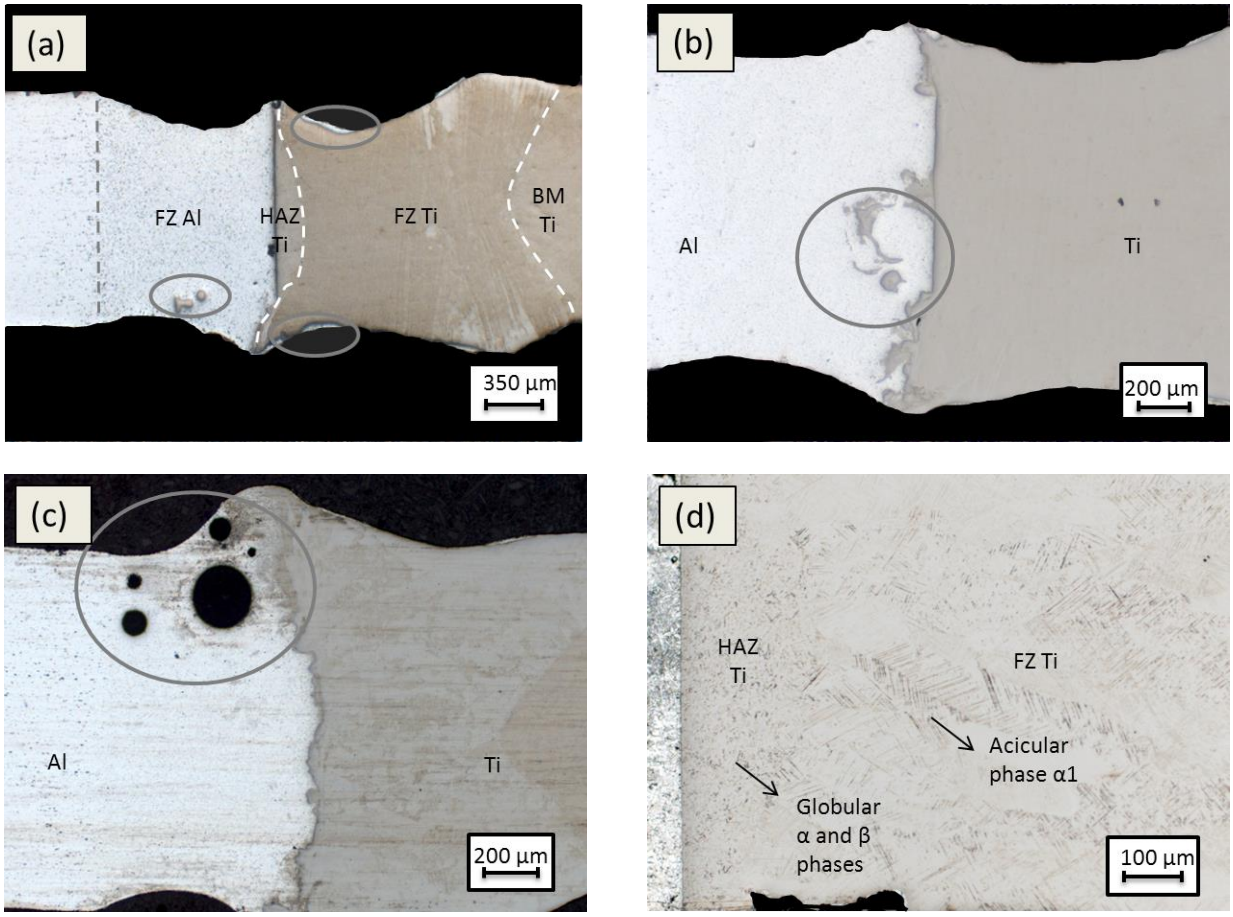

Fig. 6. Macrograph of the cross section of samples: (a) 5(1.5 kW-2m/min-0.75mm), (b) 3(1.75 kW-2m/min-0.75mm), (c) 11(1.5 kW-2.5m/min-0.5mm), (d) 6(1.5 kW-1.8m/min-0.75mm).

Figures 7(a) and 7(b) show the images detected in the region close to the interface layer through the optical microscope with a higher magnification factor (x 500). Figure 7(a) shows a typical example of a straight but serrated intermetallic layer. Lamellae of Ti were also distributed along the interface starting from the intermetallic layer towards the Al structure. This phenomena could be due to enhanced local diffusion phenomena (short-circuit like) of Ti into molten Al. Figure 7(b) shows a micrograph for which the intermetallic layer resulted to be not linear but curved. It was considered that laser beam welding produced high temperature gradient through the weld thickness, which induced uneven distribution of the reaction layer morphology.

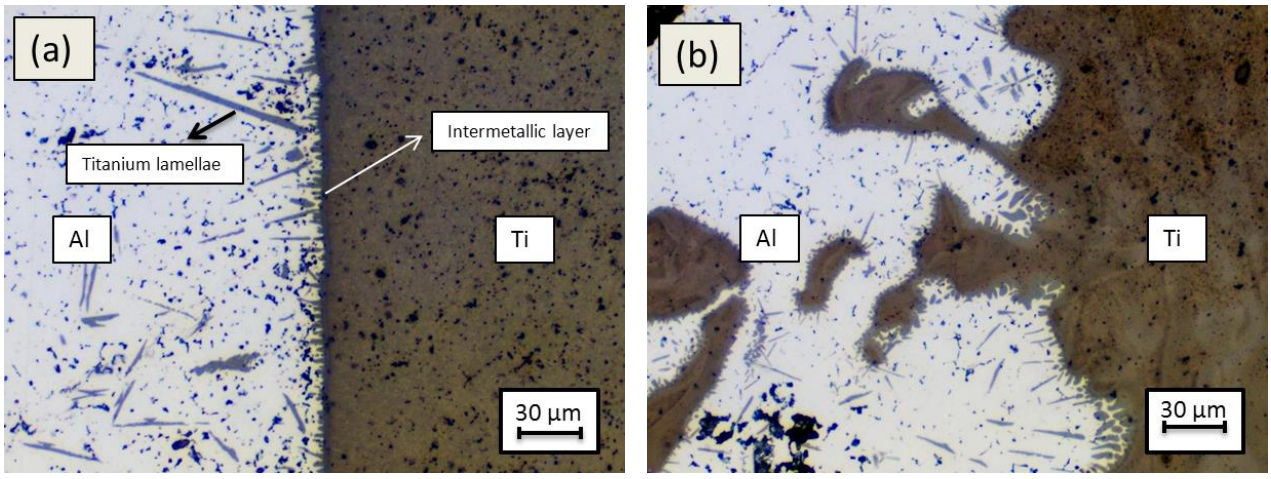

Fig. 7. Micrograph of the cross section of samples: (a) 1 (1.5 kW-1.6m/min-0.75mm) with straight intermetallic interface, (b) 9 (1.75 kW-1.6m/min-0.75mm) with irregular growth of the intermetallic layer.
.

Figure 8(a) and 8(b) shows the microstructure of two specimens observed by SEM microscopy with magnification factors of x 2000 and x 4000 respectively. Because of the reduced thickness of intermetallic (IM) layer compared with the area of the electron probe (1 µm²), it was not possible to detect the chemical content of IM. However, different EDS analysis were carried out near the interface. The localization of the zones analyzed chemically is shown in figure 8(a), while the correspondent results in term of atom percentage of the elements detected are indicated in table 6.

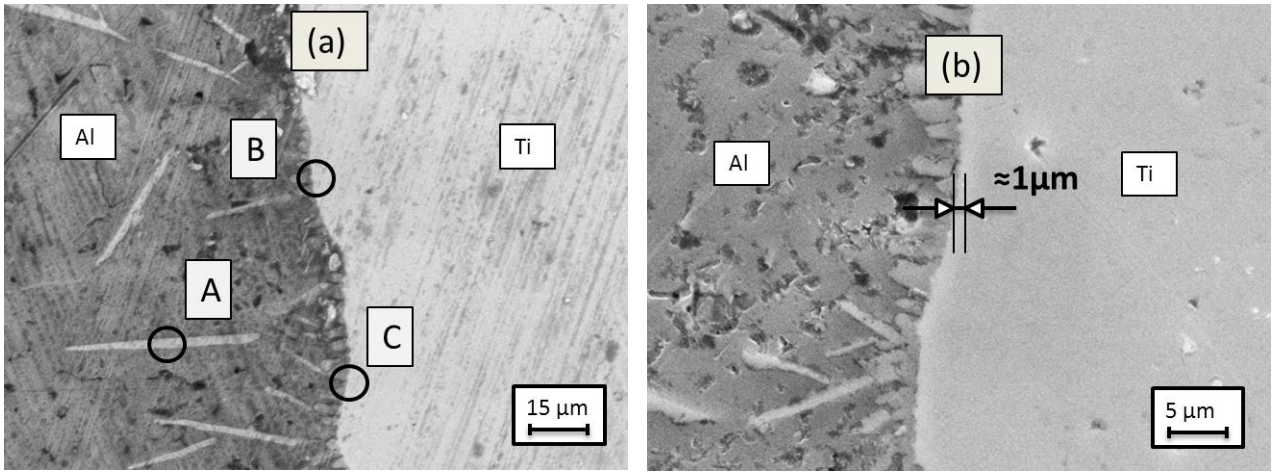

Fig. 8. Micrograph of the cross section of samples: (a) 2 (2kW-1.8m/min-0.75mm), (b) 5 (1.5kW-2m/min-0.75mm).

Tab. 6
Chemical composition (atom percentage) of the zones indicated in figure 7(b).

Micro-zone	Mg	Al	Ti	Other
A	1.2	56.6	41.6	0.6
B	1.6	68	29.9	0.5
C	2.9	63	33.6	0.5

The chemical analysis of zone A, which was assumed to correspond to a lamella, demonstrated that lamellae contain a great amount of Ti (near 40 %). Therefore, they contain Ti and Ti-Al IMC. B and C zones are made up of about 70 % of Al and 30% of Ti. This revealed that a large amount of TiAl and $TiAl_3$ were probably present but it was not possible to determine precisely the composition of IM interfacial layer due to its reduced thickness (about 1 μm). Song et al. (2013) demonstrated that the interfacial intermetallic layer is made up of TiAl, $TiAl_3$ and $TiAl_2$ and consists of 1-2 grains of intermetallic phase. Figures 9(a) and 9(b) show the SEM microstructure of the cross section of two specimens produced with different welding conditions detected with a magnification factor of x2000.

It was observed that higher lineic energies tend to increase the size of Ti-based lamellae that nucleated from the interface towards the melted Al, in the direction of the maximal thermal gradients. Moreover, also the amount of agglomerates of Ti in the Al side increases with the lineic energy. As described above, higher lineic energies also favor the formation of Ti agglomerates (Fig.7b) occluded in the Al melt-pool. This could be explained by an interfacial melting of Ti, thermo-convective flows that pushed molten Ti in the Al melt-pool, and a non-miscibility combined to large surface tension and viscosity differences, which prevented liquid mixing of Ti with Al.

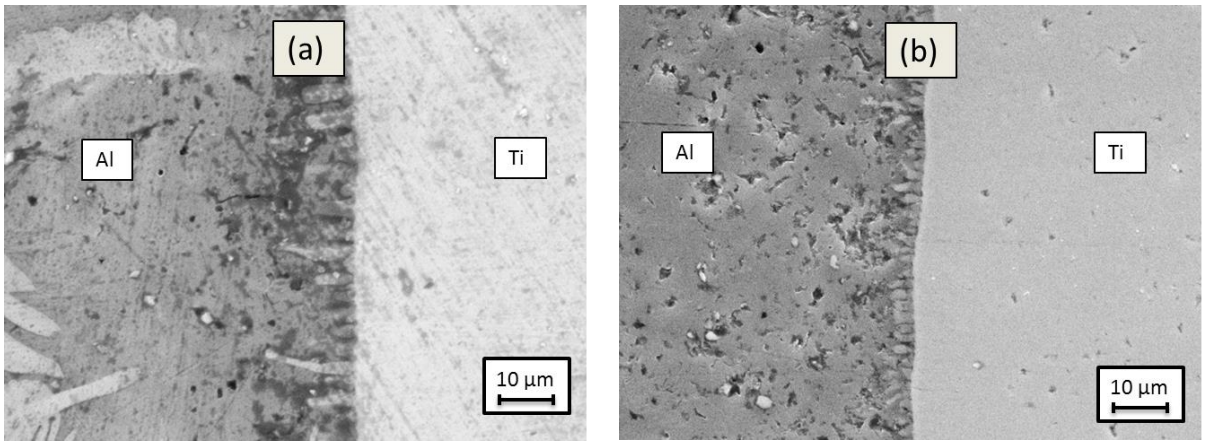

Fig. 9. Micrograph of the cross section of samples: (a) 1(1.5kW-1.6m/min-0.75mm) with lineic energy= 56.24 J/mm, (b) 5 (1.5kW-2m/min-0.75mm) with lineic energy= 45.00 J/mm.

3.3 Mechanical properties and fracture analysis

3.3.1 Micro-hardness

A micro-hardness profile carried out at the mid-thickness of an assembly is shown in figure 10. In the Al side the value of hardness was shown to increase slightly when approaching the metals interface. This may be ascribed to a grain refining in the fusion zones (FZ), with the occurrence of a fine dendritic structure. Moreover, at low distance from the interface (< 0.3 mm), molten Ti was evidenced in the FZ of Al alloy, resulting in a local hardening of Al-Mg alloy. In the Ti side, the hardness detected was greater in the FZ than in the as-received T40 (250-300 $HV_{0.2}$ versus 180-200 $HV_{0.2}$) because of the martensitic transformation. A rise of Ti hardness up to 50 % of that of the base metal (175 to 260) was registered. However, even with small loads (10-25 g), we could not detect the hardness within the intermetallic layer, which was shown to be too thin (< 3 µm) compared with the indent size. Nano-indentation tests would be necessary to investigate further the local mechanical properties of the interfacial zone.

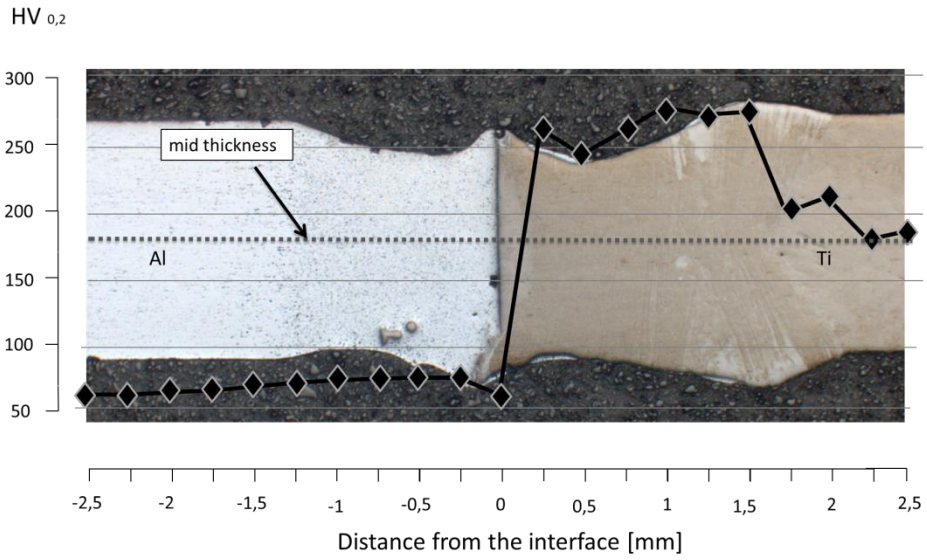

Fig. 10. Micro-hardness profile of sample 5 (1.5 kW-2m/min-0.75mm) at the mid-thickness.

3.3.2 Tensile tests

Figures 11(a), 11(b), 12(a) and 12(b) present a summary of the tensile strengths determined for the specimens of the two experimental plans (tables 4 and 5). Three specimens for each welding condition were analyzed and the mean tensile strength and elongation values were calculated and indicated with the error bars represented in the histograms. Also the lowest values and highest values are shown for each welding condition.

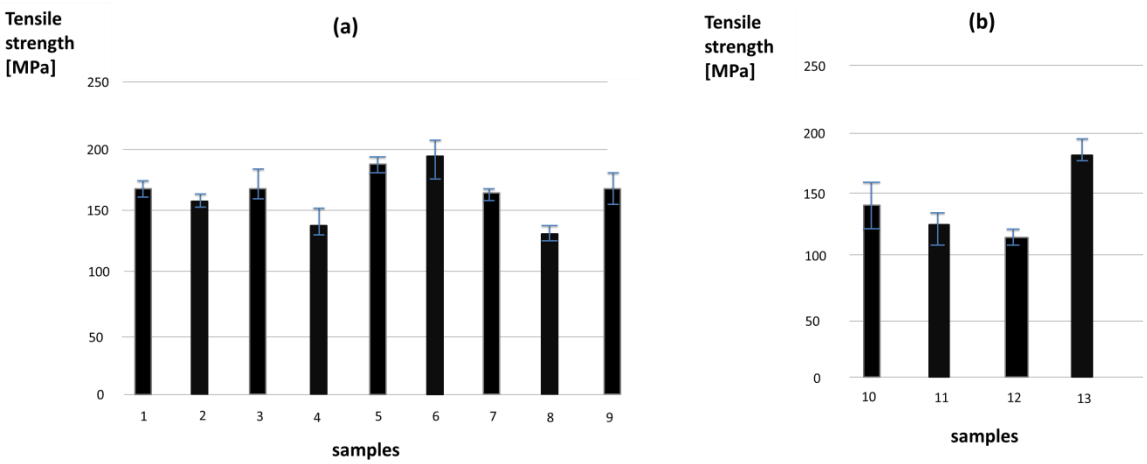

Fig. 11. Tensile strength of the samples performed in the (a) first and in the (b) second experimental plan.

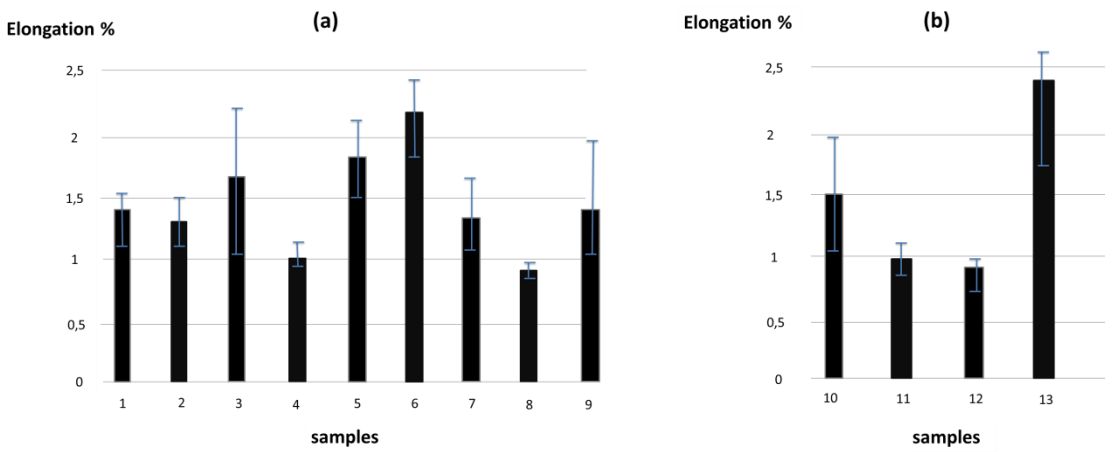

Fig. 12. Elongation % of the samples performed in the (a) first and in the (b) second experimental plan.

The mean strength value was shown to be about 160 MPa, with a great reproducibility. In spite of the fluctuations of the values of elongation the process resulted to have great robustness in term of ultimate tensile strength. The simultaneous analysis of the microstructural characteristics of welds and mechanical resistances values showed that joints for which the Ti FZ reached the interface layer tended to be less resistant mechanically. Phenomena involved near the interface, such as mixing of melted materials, alteration of the linearity of the interface and growth of Ti agglomerates and lamellae lead to a reduction of tensile strength. Referring to table 2, the tensile strength achieved for the welded joints is almost 70 % the initial strength of 5754 Al alloy. The reduction of mechanical properties is mainly due to the formation of intermetallic compounds and mixing of materials during the process. Song et al. (2013) indicated similar reduction of tensile strength for dissimilar Al-Ti joints, compared with as-received Al alloys. Considering the first experimental plan, no direct correlation could be found between tensile strengths and process conditions. Therefore, once identified the optimal range of welding parameters, the process resulted to be stable and reproducible, with a high accuracy. The second experimental plan (table 5), was implemented to try to optimize the process by reducing further the lineic energy and the offset between the interface and the center of the laser beam spot, in order to limit reductions in thickness. However, results obtained with a low offset of 0.5 mm were shown to be worse than those achieved with a laser offset of 0.75 mm. Because

of the reduction of the lineic energy P/V (J/m) due to a 3 m/min scanning speed, sample 13 was shown to be the more resistant (181 MPa). This was attributed to a better uniformity of the interface, combined with a lower interfacial mixing of materials. Last, elongation values (Fig 11(b)) globally confirm the tendency from tensile strength data: lower lineic energies promote better mechanical resistances and favor plastic behavior, maybe because of a reduction of Ti lamellae in the Al FZ. Figure 13 shows the variation of tensile strength values versus the lineic energy (defined as the ratio P/V between the output power and the welding speed).

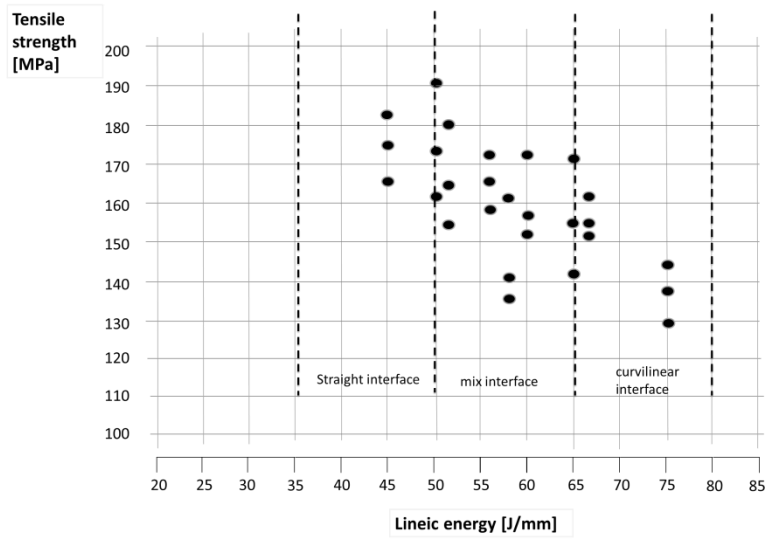

Fig. 13. Relation between the tensile strength and lineic energy adopted.

As shown in Fig.13, low lineic energy values increase the joint resistance, due to a reduced heat input that led to less alteration of the material's properties. On the other hand, higher lineic energy values resulted in a drastic reduction of mechanical resistance due to a critical melting and stirring of Ti with Al. The maximum resistance (192 MPa) was obtained for one of the lowest lineic energy values. Figures 14 and 15 show the tensile strength curves achieved for two different welding conditions, i.e. sample 4 and 6 respectively, with nearly identical lineic energies (≈ 60 J/mm).

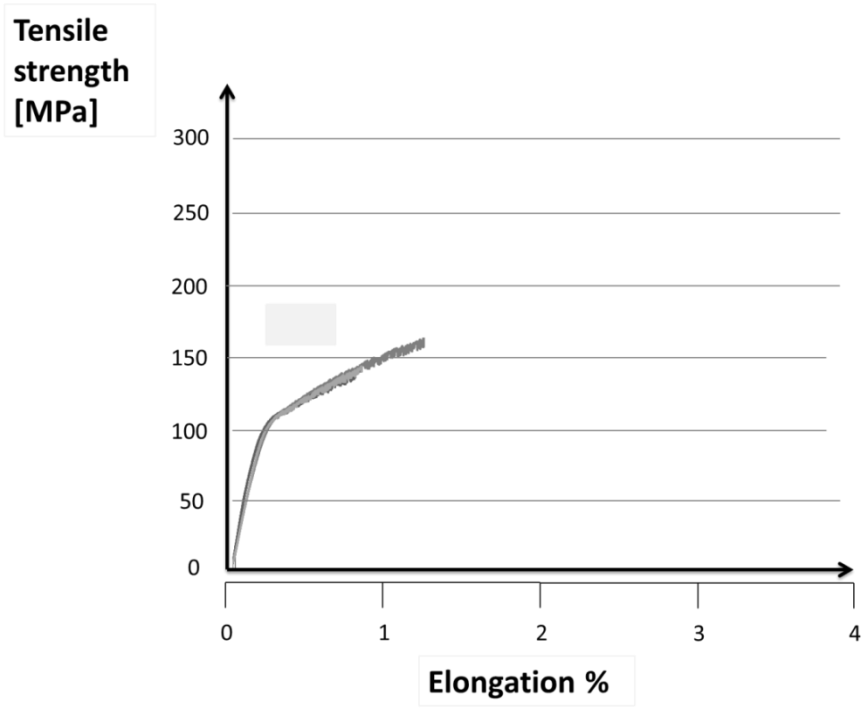

Fig. 14. Tensile test curves (A, B, C Fig. 4) for sample 4 (1.75 kW-1.8 m/min-0.75 mm-58.53J/mm).

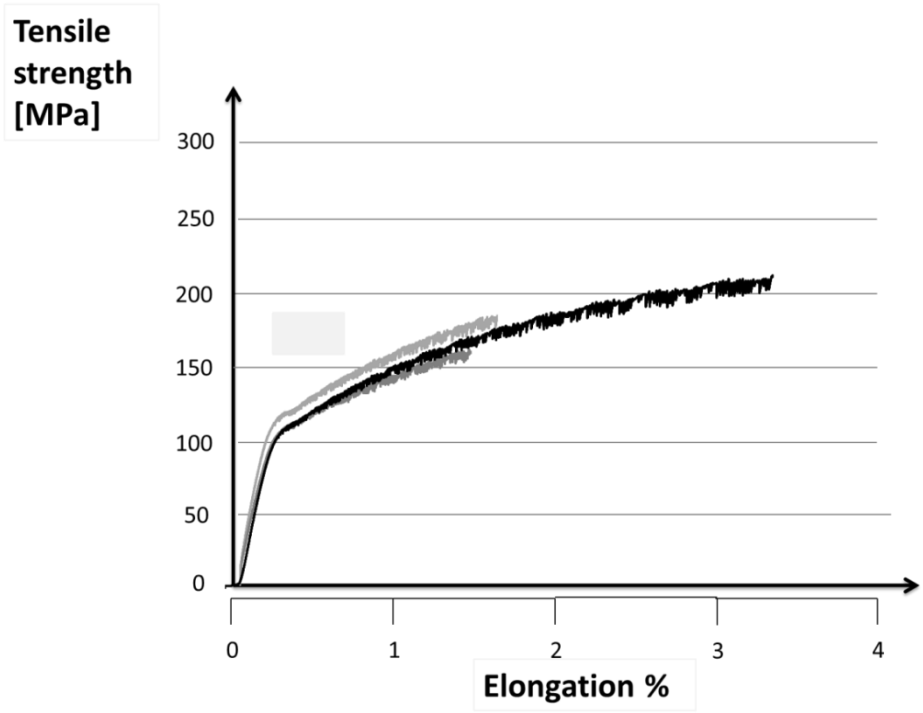

Fig. 15. Tensile test curves (A, B, C Fig. 4) for sample 6 (1.5 kW-1.8 m/min-0.75 mm-50J/mm).

The tensile test curves confirmed what has been discussed on the basis of the histograms reported, i.e. that, for each welding condition, the ultimate tensile strength is approximately constant in the entire joint, while the elongation varies significantly. The analysis of the curves presented revealed also that, in spite of the restricted difference of the values of process parameters adopted, the lineic

energy varies substantially and results present a sensitive fluctuation. Sample 6 was produced with a lower lineic energy and this led to a significant increase of mechanical properties due to the difference in morphology in proximity of the interface layer. Liquid-liquid interaction caused the growth of Ti agglomerates and lamellae that lead to a reduction of tensile strength and plasticity. The fragile rupture is revealed by the reduction in percentage elongation to fracture and yield stress in comparison with Al alloy parent metal.

3.3.3 Fracture surfaces analysis

Several fractured surfaces were analyzed with SEM. Figures 16(a) and 16(b), together with EDS local chemical analysis (Table 7), show the microstructural and chemical characteristics of fractured surfaces of two specimens performed with different welding conditions, i.e. sample 4 and sample 6. The images refers to the mid-thickness of the welds and they have a 2000x magnification.

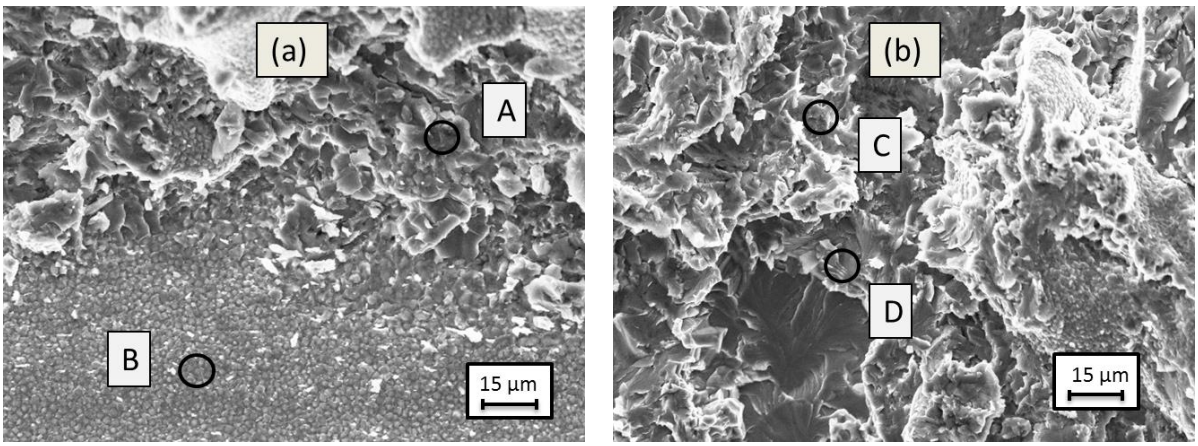

Fig. 16. Fracture surface at the mid thickness for samples (a) 4 (1.75 kW-1.8m/min-0.75mm) and (b) 6 (1.5 kW-1.8m/min-0.75mm).

Table 7
Chemical composition (atomic %, EDS) of the zones indicated in figures 16(a) and 16(b).

Micro-zone	Mg	Al	Ti	Other
A	3.7	65.4	30.6	0.3
B	1.5	79.4	18.7	0.4
C	2.6	69.6	27.5	0.3
D	1.9	20.4	77.4	0.3

Figure 16(a) refers to sample 4, performed with higher lineic energy (58 J/mm) and for which the mechanical resistance was found to be lower. On the other hand, figure 16(b) shows the fracture surface of sample 6, performed with the lower lineic energy value and for which tensile strength resulted to be higher. Zones A and C seem to contain a large amount of IMC $TiAl_3$ and TiAl. On zone B, the fracture surface contains a great amount of Al (about 75%). In this case, the fracture probably initiated in-between the IM layer and the Al alloy side. The rupture propagated from the interface towards the Al FZ. The images also revealed a brittle fracture with a cleavage morphology on a large fraction of the fracture surface. Figure 16(b) shows that fracture did not systematically occur in the axial direction (perpendicular to the loading one), but locally (zone D) could occur with a 45/60° inclination respect to the loading direction.

4. Conclusions

Dissimilar Al-Ti welding was performed by using a key-hole mode, and focusing the laser beam spot on the titanium side. In turn, a brazing effect was obtained on the aluminum side, due to solid-liquid or liquid-liquid interactions. Reproducible weld with robust properties were obtained. The following considerations were inferred from the realized study:

- The variation of lineic energy E_l and laser offset Δx determined the shape of the intermetallic layer and the geometry of the fused and heat affected zones in the cross section of welds. On one hand, joints performed with a lower E_l and larger laser offset provoked a Solid Ti / Liquid

Al interaction, and a planar intermetallic (IM) Layer. On the other hand, joints carried out with either higher E_l or lower laser offset were characterized by curved interfaces, and Al to Ti stirring due to liquid-liquid contact

- The SEM analysis revealed uniform IM layers with a thickness of about 1 μm.
- Tensile tests did not evidence a strong variation of mechanical properties with process parameters, but only a slight tensile strength decrease with increasing lineic energies. The process optimization resulted in maximal tensile strengths of about 70 % the typical mechanical resistance of the aluminum alloy. A brittle fracture was shown to occur into the intermetallic layer, with Al to Ti ratios in-between 3 ($TiAl_3$) and 1 (TiAl).
- The welding process was shown to be more stable and reproducible than with a laser beam positioned on the aluminum side, as discussed in several previous studies.

Consequently, the laser welding-brazing of T40 to A5754 was considered as a promising technique for the production of sound and robust Ti/Al assemblies.

Further investigation will concern with the nanohardness and the microstructure correlation with the welding parameters in order to optimize the mechanical properties of the weld. At a higher scale it will be interesting to heat treating the weld in order to regain some ductility to the joint.

References

Akman, E., Demir, A., Canel, T., Sınmazc¸elik, T., 2009. Laser welding of Ti6Al4V titanium alloys. Journal of materials processing technology. 209; 3705–3713.

Alfieri, V., Caiazzo, F., Sergi, V. 2013. Dissimilar joining of titanium alloy Ti-6Al-4V to aluminum alloy 2024 via laser welding. 32nd International Congress on Applications of Lasers and Electro-Optics, ICALEO 2013; Miami, FL; United States; 6-10 October.

Bondar, A.A., Witusiewicz, V.T., Hecht, U., Remez, M.V., Voblikov, V.M., Tsyganenko, N.I., Yevich, Ya. I., Podrezov, Yu. M., Velikanova, T. Ya., 2011. Structure And Properties Of Titanium–Aluminum Alloys Doped With Niobium And Tantalum. Powder Metallurgy and Metal Ceramics, Vol. 50, Nos. 7-8.

Casalino, G. , Mortello, M.A., Leo, P., Benyounis, K.Y., Olabi, A.G, 2014 Study on arc and laser powers in the hybrid welding of AA5754 Al-alloy. Materials and Design, Vol. 61; 191-198

Chen, Shuhai, Li, Liqun, Chen, Yanbin, Dai, Jingmin, Huang, Jihua, 2011. Improving interfacial reaction nonhomogeneity during laser welding–brazing aluminum to titanium. Materials and Design. 32; 4408–4416

Chen, Yanbin, Chen, Shuhai, Li, Liqun, 2010. Influence of interfacial reaction layer morphologies on crack initiation and propagation in Ti/Al joint by laser welding–brazing. Materials and Design 31; 227–233

Chen, Yuhua, Liu, Changhua, Liu, Liu, 2011 Study on the Joining of Titanium and Aluminum Dissimilar Alloys by Friction Stir Welding. The Open Materials Science Journal, 5; 256-261

Dressler, Ulrike, Biallas Gerhard, Mercado, Ulises Alfaro, 2009. Friction stir welding of titanium alloy TiAl6V4 to aluminium alloy AA2024-T3. Materials Science and Engineering A 526; 113–117.

Faller, K., Froes, F.H., 2001. The Use of Titanium in Family Automobiles: Current Trends. Titanium overview.

Haboudou, A., Peyre, P., Vannes, A.B., Peix, G., 2003. Reduction of porosity content generated during Nd:YAG laser welding of A356 and AA5083 aluminium alloys. Materials Science and Engineering. A363; 40–52

Kreimeyer, Michael, Wagner, Florian, Vollertsen, Frank, 2005. Laser processing of aluminum–titanium-tailored blanks. Optics and Lasers in Engineering. 43; 1021–1035

Kuo, Tsung-Yuan, Lin, Lin, 2006. Effects of Shielding Gas Flow Rate and Power Waveform on Nd:YAG Laser Welding of A5754-O Aluminum Alloy. Materials Transactions. Vol. 47, No. 5; 1365-1373

Lee, Ju-Jin, Nakamura, Hiroshi, Kawahito, Yousuke, Katayama, Seiji, 2013. Microstructural characteristics and mechanical properties of single mode fiber laser lap welded joint in Ti and Al dissimilar metal. Transactions of JWRI. 1; 17-21.

Luo, J-G, Acoff, V.L., 2000. Interfacial Reactions of Titanium and Aluminum during Diffusion Welding. Supplement to the welding journal, 239-243.

Miller, W.S., Zhuang a, L., Bottema, J., Wittebrood, A.J., De Smet, P., Haszler, A., Vieregge, A., 2000. Recent development in aluminium alloys for the automotive industry. Materials Science and Engineering. A280; 37–49.

Ming Gao, Cong Chen, Yunze Gu and Xiaoyan Zeng. Microstructure and Tensile Behavior of Laser Arc Hybrid Welded Dissimilar Al and Ti Alloys. Materials 2014, 7, 1590-1602; doi:10.3390/ma7031590.

Möller, F., Grden, M., Thomy, C., Vollertsen, F. Combined Laser Beam Welding and Brazing Process for Aluminium Titanium Hybrid Structures. Physics Procedia 12 (2011) 215–223.

Pastor, M., Zhao, H., Martukanitz, R.P, Debroy, T., 1999. Porosity, Underfill and Magnesium Loss during Continuous Wave Nd:YAG Laser Welding of Thin Plates of Aluminum Alloys 5182 And 5754. Welding Research Supplement. 207-216.

Song, Zhihua, Nakata, Kazuhiro, Wub, Aiping, Liao, Jinsun, 2013. Interfacial microstructure and mechanical property of Ti6Al4V/A6061 dissimilar joint by direct laser brazing without filler metal and groove. Materials Science & Engineering. A 560; 111–120

Squillace, A., Prisco, U., Ciliberto, S., Astarita, A., 2012. Effect of welding parameters on morphology and mechanical properties of Ti–6Al–4V laser beam welded butt joints. Journal of Materials Processing Technology. 212; 427– 436